ChemComm

The Power of Aluminum: Optimizing Thermoelectric Properties of the Intermetallic, Eu5+xAl3+ySb6

Journal:	*ChemComm*
Manuscript ID	CC-COM-03-2025-001165.R2
Article Type:	Communication

ChemComm

COMMUNICATION

The Power of Aluminum: Optimizing Thermoelectric Properties of the Intermetallic, $Eu_{5+x}Al_{3+y}Sb_6$

Received 00th January 20xx,
Accepted 00th January 20xx

DOI: 10.1039/x0xx00000x

Luis Garay,[1] Leah Borgsmiller,[2] G. Jeffrey Snyder,[2] and Susan M. Kauzlarich[1*]

$Eu_{5.08}Al_3Sb_6$ can be described as a pseudo rock salt-like "$(Eu/Al_4)Sb$" structure. The polycrystalline synthesis of $Eu_{5+x}Al_{3+y}Sb_6$ was optimized. The compositions exhibit n-type transport behavior, ultra-low thermal conductivity, and a high Seebeck coefficient. The $Eu_{5.08}Al_4Sb_6$ shows a promising *zT* of 0.8 at a temperature of 873 K.

Intermetallics have gathered attention as a class of compounds because they provide insight into diverse studies of chemical composition, atomic structure, electronic structure, and physical properties.[1,2] These compounds can be binary, ternary, or poly-metallic phases composed of metals or a combination of metals and metalloids in different stoichiometric ratios.[3] There are three categories of intermetallic phases defined by their corresponding ratio of valence electrons per atom (e/a): Hume-Rothery phases, $1 \leq (e/a) \leq 2$; polar intermetallics, $1.2 \leq (e/a) \leq 4$; Zintl phases $(e/a) \geq 4$.[1,4–6] Polar intermetallics can exhibit the unique combination of chemical and structural features seen in both Hume-Rothery and Zintl phases based on electron counting.[2,5] Like the Zintl counterparts, the complexity of polar intermetallic crystal structures, along with defects, can make them good candidates for thermoelectric materials.[2,7,8]

Thermoelectric materials are essential renewable energy sources due to their niche function of converting waste heat to electrical energy through the Seebeck effect. The Seebeck effect involves the movement of carriers (holes or electrons) when a thermal gradient is applied to produce a voltage.[2,7,9] Typically, two semiconductors, a p-type, whose majority carriers are holes, and an n-type, whose majority carriers are electrons, are connected in series perpendicular to the gradient, and a voltage is produced.[7,9] These materials can be used as thermoelectric generators (TEGs), which work similarly to heat engines and can be used for power plants, automotive, or deep space exploration. Thermoelectric materials with high efficiency and optimal performance are most appropriate for industrial application devices. Typically, the performance of these thermoelectric materials is governed by their dimensionless figure of merit known as *zT* (eq 1):

$$zT = \frac{\alpha^2 T}{\rho(k_l + k_e)} \qquad \text{eq 1}$$

where the following variables α, T, ρ, κ_l, and κ_e are the Seebeck coefficient, absolute temperature, electrical resistivity, and the lattice and electrical segments of the thermal conductivity, respectively. These variables are interconnected based on carrier concentration.[7] Compositional tuning is an approach to fine-tune the carrier concentration, as structural components can introduce more energy levels that can either donate or accept electrons, improving electrical conductivity. This approach has shown success in the ultralow lattice thermal conductivity material, $Cu_{2.83-x}Bi_{10}Se_{16}$, where both DFT simulations and experimental measurements demonstrate the thermoelectric performance enhancement by controlling the amount of Cu in the material.[10] Composition makes a significant impact on the low lattice thermal conductivity found for TiNiSn half-Heusler phases, which is attributed to the excess Ni in the structure.[11] Highly symmetric semiconductors, such as SnTe, which adopt a NaCl structural motif, possess promising, capable mid-temperature thermoelectric properties that are credited to populating the Sn vacancies.[12] SnTe with Pb alloying exhibited a high Seebeck coefficient similar to PbTe because of its complex electronic structure, increased carrier concentration, and low thermal conductivity.[12,13]

The crystal structure of the compound, $Eu_{5.08}Al_3Sb_6$, is provided in Fig. 1. Single crystal diffraction and electron microscopy reveal a pseudo rock salt structural motif, crystallizing in the monoclinic C2/*m* space group.[4,14] This simple yet complex unit cell is attributed to the partially occupied Al_4 cluster in the center of the octahedral unit at the corners and centered on the (001) plane of the unit cell, as shown in Fig. 1. As a result of its valence electron to atom ratio (e/a) of 3.5 and variable composition, the $Eu_{5.08}Al_3Sb_6$ compound is classified as a polar intermetallic.[4,14] Additionally, electrical resistivity measurements as a function of temperature show semimetallic behavior with a room temperature electrical resistivity value of 2 mΩ · cm.[14] The electronic structure calculations provide insight into the presence of disordered Al clusters and the significant Al deficiency within the tetrahedra due to the

Affiliations
[1]Department of Chemistry, University of California, Davis, CA 95616, United States
[2]Department of Materials Science and Engineering, Northwestern University, Evanston IL 60208, United States
**Corresponding author's email: smkauzlarich@ucdavis.edu*
† Footnotes relating to the title and/or authors should appear here.
Electronic Supplementary Information (ESI) available: Detailed experimental description, X-ray powder diffraction patterns and refinement, TG/DSC, SEM/EDS, Calculated lattice thermal conductivity. See DOI: 10.1039/x0xx00000x

antibonding Al–Sb character near the Fermi level.[14] Based on the proposed band structure, the hypothetical $Eu_5Al_4Sb_6$ compound is considered semimetallic. This characterization is consistent with the presented properties. Single crystals of the solid solution, $Eu_{5-x}Sr_xAl_3Sb_6$, indicated that this intermetallic has a phase width with variable composition of Eu/Sr and Al.[4] Because of the published electronic structure, a high Seebeck value is expected, attributed to multi-valley orbital degeneracy. We also expect low thermal conductivity based on the structural complexity.

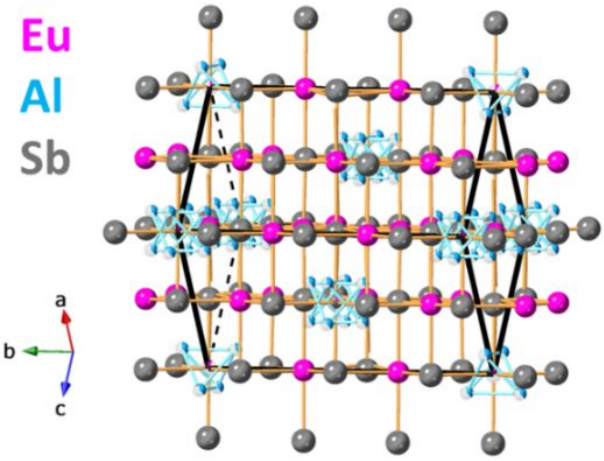

Fig 1. A view of the unit cell of the $Eu_{5.08}Al_3Sb_6$ shows the pseudo rock salt framework, with Eu, Al, and Sb atoms shown in pink, blue, and grey, respectively.

Polycrystalline metallurgical synthesis was employed and optimized using binary precursors, as described in the ESI‡. Plots of powder X-ray diffraction of the binary precursors are provided in the ESI‡, Fig. S1, with Rietveld refinement parameters in Table S1. The powder diffraction patterns of $Eu_{5+x}Al_{3+y}Sb_6$ (with nominal compositions of x = 0.00, 0.08; y = 0.30, 1.00) are provided in Fig. 2; the lattice parameters are provided in Table 1, and selected Rietveld refinement and statistics are provided in the ESI‡, Fig. S2, and Table S2. The nominal compositions $Eu_{5.08}Al_{3.3}Sb_6$, $Eu_{5.08}Al_4Sb_6$, and $Eu_5Al_4Sb_6$ are phase pure by PXRD, EDS, and Rietveld Refinement provided in the ESI‡, Figs S2, S4 and S5. Compositions prepared as x = 0.00, y = 0.00, and 0.30 exhibit an impurity phase identified as Eu_3AlSb_3. The calculated atomic percentages for the Eu_3AlSb_3 composition are 42.9% (Eu), 14.2% (Al), and 42.9% (Sb), while for $Eu_{5.08}Al_3Sb_6$, the atomic percentages are 36.1% (Eu), 21.3% (Al), and 42.6% (Sb). The proximity in ternary space of the Eu_3AlSb_3 impurity to that of $Eu_{5.08}Al_3Sb_6$ requires an excess of Al and Eu to obtain a phase-pure sample. The possible presence of excess Al at the grain boundary was investigated with differential scanning calorimetry (DSC), provided in the ESI‡, **Fig. S3**. There is no evidence for excess Al in the samples.

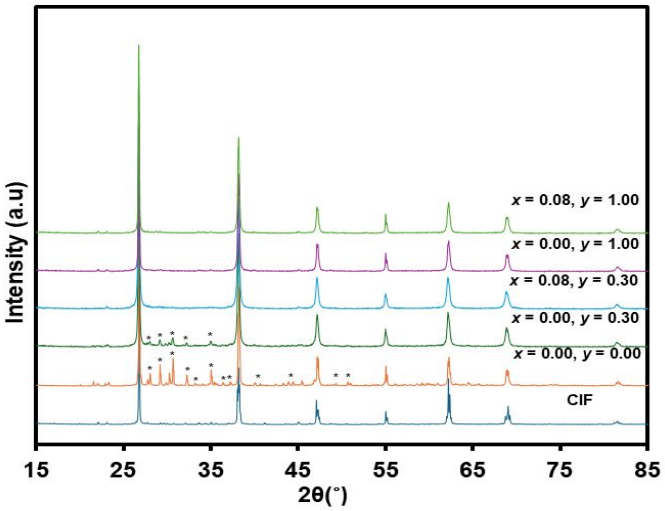

Fig 2. PXRD patterns of $Eu_{5+x}Al_{3+y}Sb_6$ (x = 0.00, 0.08; y = 0.30, 1.00) samples compared to the PXRD calculated from the single crystal CIF of the published structure $Eu_{5.08}Al_3Sb_6$ (x = 0.08, y = 0.00; bottom dark blue). The asterisks indicate impurity peaks of an unreported Eu_3AlSb_3 phase, consistent with the Ba_3AlSb_3 structure type.

Table 1. Lattice Parameters from Rietveld Refinement of $Eu_{5+x}Al_{3+y}Sb_6$ (x = 0.00, 0.08 and y = 0.30, 1.00)

Lattice Parameters	$Eu_{5.08}Al_{3.3}Sb_6$	$Eu_{5.08}Al_4Sb_6$	$Eu_5Al_{3.3}Sb_6$	$Eu_5Al_4Sb_6$
a (Å)	8.1711(17)	8.1618(6)	8.1660(12)	8.1618(5)
b (Å)	14.117(3)	14.108(1)	14.116(2)	14.108(1)
c (Å)	8.1845(17)	8.1780(5)	8.1775(13)	8.1761(5)
β (°)	109.379(8)	109.356(5)	109.383(7)	109.370(5)
Volume (Å^3)	890.6(3)	888.5(1)	889.2(2)	888.2(1)

Secondary electron images and elemental analysis confirm the pellets' phase purity and homogeneity and are provided in the ESI‡, **Figs S4-S5**. The nominal compositions of the polycrystalline samples versus the calculated composition obtained from EDS are provided in the ESI‡, **Table S3.** The addition of the small amounts of Al is consistent with the increased Al composition calculated from the EDS. The transport properties of the four samples are provided in **Fig. 3**. The carrier concentration (**Fig. 3a**) increases by two orders of magnitude at 300 K as the Al content increases from 1.10 x 10^{18} cm^{-3}(y = 0.30) to 2.10 x 10^{20} cm^{-3} (y = 1.00). The increase in carrier concentration is attributed to the contribution of the additional electrons from the Al cluster to the conduction band.[14] Therefore, adjusting the stoichiometry of Al in this system plays a role in fine-tuning electrical transport properties via carrier concentration. Contribution from minority carriers may cause the increase in the carrier concentration above 600 K.[15] **Fig. 3b** shows the Hall carrier mobility, and all four samples follow a similar trend between 298 K and 450 K, where the mobility decreases as temperature increases. This decrease in mobility as a function of temperature is seen in metallic systems and can be attributed to increased phonon scattering at higher temperatures. However, similar to the Half-Heusler phase $ScNiSb_{1-x}Te_x$, mobility increases at higher temperatures and is

attributed to a mix of scattering mechanisms such as ionized impurity ($\mu_H \propto T^{3/2}$) and grain boundary scattering ($\mu_H \propto \exp[-1/T]$).[15] Temperature-dependent resistivity is shown in **Fig. 3c**, where $Eu_{5.08}Al_{3.30}Sb_6$ and $Eu_5Al_{3.30}Sb_6$ show high room temperature resistivity of 297 mΩ cm and 429 mΩ · cm, respectively. These values are lower than those of semiconductor Zintl compounds with similar elements, *e.g.,* $Eu_5Al_2Sb_6$ (ρ(300 K) = 1.4(1) Ω · cm) and $Eu_{14}AlSb_{11}$ (ρ(300 K) ~ 0.4 Ω · cm).[16,17] The temperature-dependent electrical resistivity for the 3.3 Al-containing compounds decreases as temperature increases from 300 to 700 K, which is typical for degenerate semiconductors. $Eu_{5.08}Al_4Sb_6$ and $Eu_5Al_4Sb_6$ show much lower resistivity with ρ_{300} at 10.0 mΩ · cm and 9.0 mΩ · cm, respectively. The electrical resistivity slightly increases as a function of temperature, which is expected for metallic or heavily doped semiconducting systems.[8,16,18] The temperature-dependent Seebeck coefficients indicative of n-type transport behavior, shown in **Fig. 3d**, indicate the predominant carriers are electrons. The series follows a similar temperature-dependent trend based on the corresponding carrier concentration and mobility. $Eu_5Al_4Sb_6$ has a Seebeck coefficient of -247.4 μV/K at a temperature of 723 K. The maximum Seebeck coefficient for $Eu_{5.08}Al_4Sb_6$ is -211.9 μV/K at 723 K, whereas samples with a lower Al content of 3.3 exhibit higher Seebeck coefficients of -270.0 and -276.5 μV/K at the same temperature. The Seebeck values of the samples with lower Al content show an upturn at around 600 K, suggesting the onset of minority carriers and a narrow-band semiconductor.[3,12,13] Adding more Al and increasing Eu content shifts the upturns to higher temperatures.

In the published band structure, the experimental composition $Eu_{5.08}Al_3Sb_6$ corresponds to a Fermi level located at 1.2 eV, consistent with approximately 49 valence electrons—slightly fewer than the 52 electrons in $Eu_5Al_4Sb_6$, where the Fermi level is set at 0 eV.[14] The slight excess of Eu in $Eu_{5.08}Al_4Sb_6$ likely acts as an effective n-type dopant, shifting the Fermi level further into the conduction band. While stoichiometric $Eu_5Al_4Sb_6$ lies near a semimetal-to-semiconductor boundary—with a Fermi level close to a small band gap or overlap—the doped $Eu_{5.08}Al_4Sb_6$ composition, with its higher electron count, is expected to be more conductive.[19] The reported band structure at E = 0 eV shows at least two bands likely contributing to the high Seebeck values and low electrical resistivity in the $Eu_{5+x}Al_{3+y}Sb_6$ series: one near the X point, and another along the E–M path. In semi-metallic systems like the NiTZ half-Heusler alloys, enhanced thermoelectric performance has been attributed to multiple band contributions, specifically heavy and light bands. The heavy bands support higher Seebeck coefficients, while the light bands enable higher carrier mobility.[20,21] For other half-Heusler systems, such as $TiCo_{0.85}Fe_{0.15}Sb_{1-x}Sn_x$, band convergence has proven to be an effective strategy, producing promising room-temperature Seebeck values of 140–180 μV/K.[22] Similarly, ZrNiSn, a semi-metallic Half-Heusler compound, exhibits a high negative Seebeck coefficient of around −250 μV/K. Upon Nb doping in $Zr_{1-x}Nb_xNiSn$, the Seebeck coefficient systematically decreases as the carrier concentration increases, a trend also observed in Sb-doped ZrNiSn.[23] The behavior of $Eu_{5+x}Al_{3+y}Sb_6$ is similar to that of other correlated or multiband semi-metallic systems, particularly among half-Heusler compounds, where sharp density-of-states features, multiband conduction, and pseudogap-like behavior lead to enhanced thermopower even in metallic or near-metallic regimes. Similar high negative Seebeck coefficients are also observed in high-symmetry rock salt structures like PbTe, where high band degeneracy plays a key role in enhancing thermopower.[3,13] Experimental results—such as reduced resistivity, increased carrier concentration, and a modest decrease in the magnitude of the Seebeck coefficient with added Eu and Al—support this interpretation.

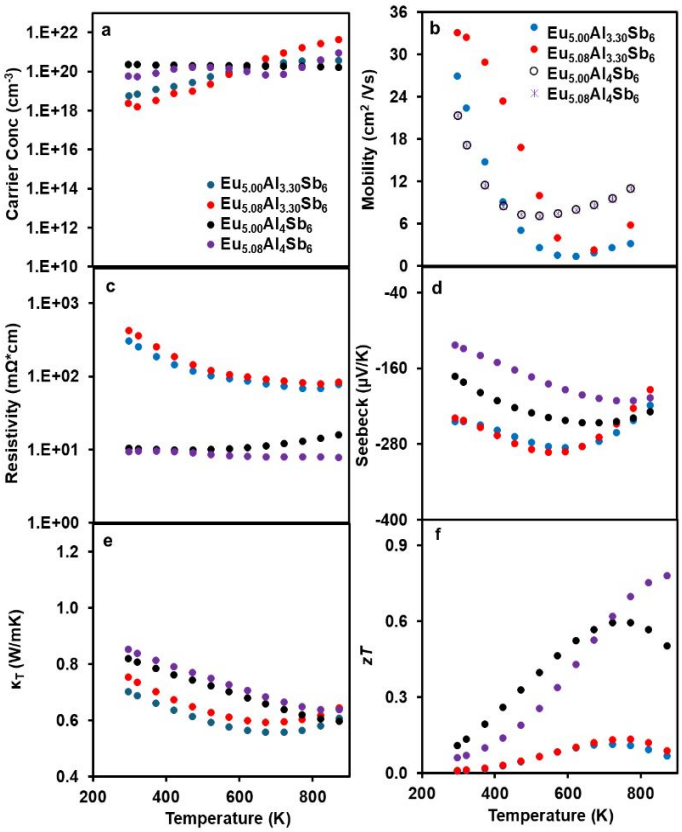

Fig 3. Temperature-dependent a) charge carrier concentration determined via the Hall effect b) charge carrier mobility, c) electrical resistivity, d) Seebeck coefficient e) total thermal conductivity, and f) thermoelectric figure of merit as a function from 300 to 800 K for $Eu_{5+x}Al_{3+y}Sb_6$ (x = 0.00, 0.08 and y = 0.30, 1.00).

The total thermal conductivity values shown in Fig. 3e are low for all compounds, < 0.9 W/m · K. The lattice thermal conductivity is shown in ESI‡, Fig. S6. Low thermal conductivity is expected since this compound has structural disorder and contains heavy atoms. The lattice contribution is more evident in the y = 1.00 samples. The incorporation of a Lorenz number effectively diminishes the lattice thermal conductivity to zero at 600 K. Metals exhibiting complex crystal structures, such as $Ba_{0.08}La_{0.55}Yb_{0.04}Co_4Sb_{12}$, Mo_3Sb_{77}, and $La_{3-x}Te$, demonstrate Lorenz factors that are 20% to 40% lower than the conventional electron value.[8] Notably, exceptionally low Lorenz values have been observed in $Yb_9Mn_{4.2-x}Zn_xSb_9$ and $Eu_9Cd_4Sb_9$, which are typically associated with nondegenerate semiconductors rather than complex metallic compounds.[8,18] Several factors, including intrinsic defects such as phonon scattering from point defects, the presence of aluminum at grain boundaries, and disorder within the system, contribute to the reduction in thermal conductivity.[16] The thermoelectric figure of merit (Fig. 3f) is low

for the compositions $Eu_5Al_{3.3}Sb_6$ and $Eu_{5.08}Al_{3.3}Sb_6$, reaching a peak value of 0.1 at 773 K. However, given the high carrier concentration and Seebeck, along with the ultralow thermal conductivity for the compositions $Eu_{5.08}Al_4Sb_6$ and $Eu_5Al_4Sb_6$, a zT_{max} of 0.8 at 873 K and 0.6 at 773 K was achieved, respectively.

A polycrystalline synthesis to prepare phase-pure $Eu_{5.08}Al_3Sb_6$ was developed, and a compositional study was presented. Both Al and Eu content impact the purity and thermoelectric properties of this newly identified semimetallic n-type material. This n-type intermetallic exhibits low thermal conductivity (< 0.9 W/m · K) and high negative Seebeck values. Carrier concentration and electrical resistivity are controlled with composition, shifting the total electron count from about 49 to 52 e^-/formula unit. The high Seebeck coefficient is attributed to the high symmetry of the pseudo rock-salt structure and multi-valley band degeneracy. In contrast, the low thermal conductivity is linked to structural features within the material, as noted in Fig. 1.[9] The structural disorder of the Al cluster can be considered as point defects (along with the corresponding vacancies and Eu atom substitution). These defects serve as scattering centers, contributing to the material's low thermal conductivity. Incorporating additional Al and Eu leads to a better thermoelectric figure of merit, *zT,* with the nominal composition of $Eu_{5.08}Al_4Sb_6$ showing promise for further improvement.

This work was supported by the National Science Foundation (NSF), DMR-2335203. SEM/EDS data were obtained from the Advanced Materials Characterization and Testing Laboratory (AMCaT) supported by NSF DMR-1725618 at the University of California, Davis. L.B. is supported by the National Science Foundation Graduate Research Fellowship Program under Grant No. DGE-1842165. Any opinions, findings, conclusions or recommendations expressed in this material are those of the authors and do not necessarily reflect the views of the National Science Foundation. This work was performed under the financial assistance of Award No. 70NANB19H005 from U.S. Department of Commerce, National Institute of Standards and Technology as part of the Center for Hierarchical Materials Design (CHiMaD).

Data availability

Electronic Supplementary Information (ESI) available: Detailed experimental description, X-ray powder diffraction patterns and refinement, TG/DSC, SEM/EDS, Calculated lattice thermal conductivity.

Conflicts of interest

There are no conflicts of interest to declare.

Notes and References

(1) Q. Lin and G. J. Miller, *Acc. Chem. Res.*, 2018, **51**, 49–58.

(2) S. M. Kauzlarich, *Chem. Mater.*, 2023, **35**, 2303–2313.

(3) Z. Chen, B. Ge, W. Li, S. Lin, J. Shen, Y. Chang, R. Hanus, G. J. Snyder and Y. Pei, *Nat. Commun.*, 2017, **8**, 13828.

(4) L. Garay, J. L. Gonzalez Jimenez, J. C. Fettinger, S. O. Gunther, J. A. Branson, S. G. Minasian, W. Xie and S. M. Kauzlarich, *Inorg. Chem.*, 2025, **64**, 1024–1034.

(5) S. Lotfi and J. Brgoch, *Chem. - A Eur. J.*, 2020, **26**, 8689–8697.

(6) S. Lotfi, R. Arrieta, G. G. C. Peterson, P. Delgado and J. Brgoch, *ACS Org. Inorg. Au*, 2022, **2**, 318–326.

(7) G. J. Snyder and E. S. Toberer, *Nat. Mater.*, 2008, **7**, 105–114.

(8) S. Ohno, A. Zevalkink, Y. Takagiwa, S. K. Bux and G. J. Snyder, *J. Mater. Chem. A*, 2014, **2**, 7478–7483.

(9) S. Iwanaga, E. S. Toberer, A. LaLonde and G. J. Snyder, *Rev. Sci. Instrum.*, 2011, **82**, 63905.

(10) Z. Ye, W. Peng, F. Wang, A. Balodhi, R. Basnet, J. Hu, A. Zevalkink and J. Wang, *ACS Appl. Energy Mater.*, 2021, **4**, 11325–11335.

(11) T. Zilber, S. Cohen, D. Fuks and Y. Gelbstein, *J. Alloys Compd.*, 2019, **781**, 1132–1138.

(12) H. Pang, Y. Qiu, D. Wang, Y. Qin, R. Huang, Z. Yang, X. Zhang and L.-D. Zhao, *J. Am. Chem. Soc.*, 2021, **143**, 8538–8542.

(13) Y.-L. Pei and Y. Liu, *J. Alloys Compd.*, 2012, **514**, 40–44.

(14) A. He, Z. Shen, H. Wang, W. Xie, Z. Wang, L. Garay, J. C. Fettinger, R. P. Hermann, Y. Zhu, V. Taufour and S. M. Kauzlarich, *Chem. Mater.*, 2022, **34**, 5009–5019.

(15) K. Ciesielski, I. Wolańska, K. Synoradzki, D. Szymański and D. Kaczorowski, *Phys. Rev. Appl.*, 2021, **15**, 044047.

(16) M. Radzieowski, T. Block, T. Fickenscher, Y. Zhang, B. P. T. Fokwa, O. S. Janka, *Mater. Chem. Front.*, 2017, **1**, 1563–1572.

(17) A. C. Payne, M. M. Olmstead, S. M. Kauzlarich and D. J. Webb, *Chem. Mater.*, 2001, **13**, 1398–1406.

(18) N. Kazem, J. V. Zaikina, S. Ohno, G. J. Snyder and S. M. Kauzlarich, *Chem. Mater.*, 2015, **27**, 7508–7519.

(19) S. Guo, S. Anand, M. K. Brod, Y. Zhang and G. J. Snyder, *J. Mater. Chem. A*, 2022, **10**, 3051–3057.

(20) R. J. Quinn and J.-W. G. Bos, *Mater. Adv.*, 2021, **2**, 6246–6266.

(21) D. R. Jaishi, N. Sharma, B. Karki, B. P. Belbase, R. P. Adhikari and M. P. Ghimire, *AIP Adv.*, 2021, **11**, 25304.

(22) A. K. Verma, K. K. Johari, P. Dubey, D. K. Sharma, S. Kumar, S. R. Dhakate, C. Candolfi, B. Lenoir and B. Gahtori, *ACS Appl. Mater. Interfaces*, 2023, **15**, 942–952.

(23) K. K. Johari, R. Bhardwaj, N. S. Chauhan, S. Bathula, S. Auluck, S. R. Dhakate and B. Gahtori, *ACS Appl. Energy Mater.*, 2021, **4**, 3393–3403.

Electronic Supplementary Information (ESI) available: Detailed experimental description, X-ray powder diffraction patterns and refinement, TG/DSC, SEM/EDS, Calculated lattice thermal conductivity.